JACS
JOURNAL OF THE AMERICAN CHEMICAL SOCIETY

Communication

pubs.acs.org/JACS

Controllably Interfacing with Metal: A Strategy for Enhancing CO Oxidation on Oxide Catalysts by Surface Polarization

Yu Bai,[†] Wenhua Zhang,[†] Zhenhua Zhang,[†] Jie Zhou, Xijun Wang, Chengming Wang, Weixin Huang,* Jun Jiang,* and Yujie Xiong*

Hefei National Laboratory for Physical Sciences at the Microscale, Collaborative Innovation Center of Chemistry for Energy Materials, School of Chemistry and Materials Science, and CAS Key Laboratory of Materials for Energy Conversion, University of Science and Technology of China, Hefei, Anhui 230026, P. R. China

Supporting Information

ABSTRACT: Heterogeneous catalysis often involves charge transfer from catalyst surface to adsorbed molecules, whose activity thus depends on the surface charge density of catalysts. Here, we demonstrate a unique solution-phase approach to achieve controllable interfacial lengths in oxide-metal hybrid structures. Resulting from their different work functions, surface polarization is induced by the Ag-CuO interface and acts to tailor the surface charge state of CuO. As a result, the designed hybrid catalysts exhibit enhanced intrinsic activities in catalyzing CO oxidation in terms of apparent activation energy, as compared with their counterparts. Moreover, the CO conversion rate can be enhanced by maximizing the Ag-CuO interfacial length and thus the number of active sites on the CuO. This work provides a new strategy for tuning catalytic performance by controlling interface in hybrid catalysts.

Heterogeneous catalysis represents an important route to facilitate various reactions such as CO oxidation, in which charge transfer typically occurs between adsorbed species and catalyst surface. The efficiency of such charge transfer is thus dependent on the surface charge density of catalysts, opening possibilities to tuning catalytic performance.[1−3] In the past years, tremendous efforts have been made to control the surface facets of catalytic materials;[3−7] however, it remains a grand challenge to arbitrarily tailor the surface charge state of these solid materials.

To maneuver the charge state, surface polarization has been identified as a general method by modifying the electronic structures of materials.[8−10] In hybrid structures, the variation in material work functions may cause polarization at the interface of components.[9,10] In traditional two-dimensional models, the interface polarization can drive charges to reach surface and thereby sustain surface polarization, when the layer thickness of catalytic materials is confined at the atomic level.[9,10] However, the fabrication of such structures generally requires expensive atomic layer deposition (ALD) technique. Alternatively, it represents a more cost-effective approach that hybrid structures are constructed by stacking the nanocrystals with different electronic structures to form interfacial lines for catalytic reactions.[11] To exploit practical applications, however, it is imperative to fundamentally prove whether surface polarization can effectively take place in such nanocrystal-based systems. Technically, it is also needed to develop methods for *in situ* growing high-quality interface (e.g., single crystal) to facilitate the surface polarization, as well as controlling the interfacial lengths to tune catalytic activities.

Here, we report the controllable growth of Cu_2O layers (partial coverage with varied interfacial lengths versus full coverage) on Ag nanoplates, which offers an excellent platform for investigating the effect of surface polarization on CO oxidation. This hybrid combination is chosen for our study due to two reasons: (1) Ag nanoplates have a flat surface allowing the precise deposition of Cu_2O in solution phase, and the possibility of growing Cu_2O on other noble metals has been previously validated;[12,13] and (2) Cu_2O can be converted into a stable catalyst for CO oxidation; CuO after a simple oxidation step.[7] Based on this synthetic approach, we find out that the catalytic CO conversion rates are strongly correlated to the interfacial lengths between the resulted CuO and the Ag, providing a versatile knob for tuning catalytic performance. More importantly, this interface enables significantly lower activation energy as compared with bare CuO, making use of the surface polarization mechanism.

We first synthesize the template substrates of Ag nanoplates by following a hydrothermal process.[14] The Ag nanoplates have edge lengths of 500−900 nm and {111} facets exposed on surface (Figure S1). To controllably coat single-crystal Cu_2O on the edges, we intentionally manipulate two parameters: (1) concentration of Cu precursor $CuCl_2$ is maintained low so as to supply insufficient Cu stock for Cu_2O growth; and (2) poly(vinylpyrrolidone) (PVP) is used as a capping agent to promote the formation of Cu_2O{111} flat surface (aligning to the Ag{111}), as the PVP is known to be selectively adsorbed on the {111} facets of Cu_2O nanocrystals.[15] As a result, Cu_2O is partially deposited on the area close to the edges of Ag nanoplates, leaving the central part uncovered (Figure 1a,b). This growth mode leads to the formation of a unique Ag-Cu_2O hybrid structure with both Ag and Cu_2O surface exposed.

Scanning and transmission electron microscopy (SEM and TEM) images show that the average interfacial length between Ag and Cu_2O is 1550 ± 500 nm (namely, partial coverage I). It should be noted that the resulted sample has a relatively broad distribution in interfacial lengths (see Figure S2) resulting from

Received: June 22, 2014
Published: October 8, 2014

dx.doi.org/10.1021/ja506269y | J. Am. Chem. Soc. 2014, 136, 14650−14653

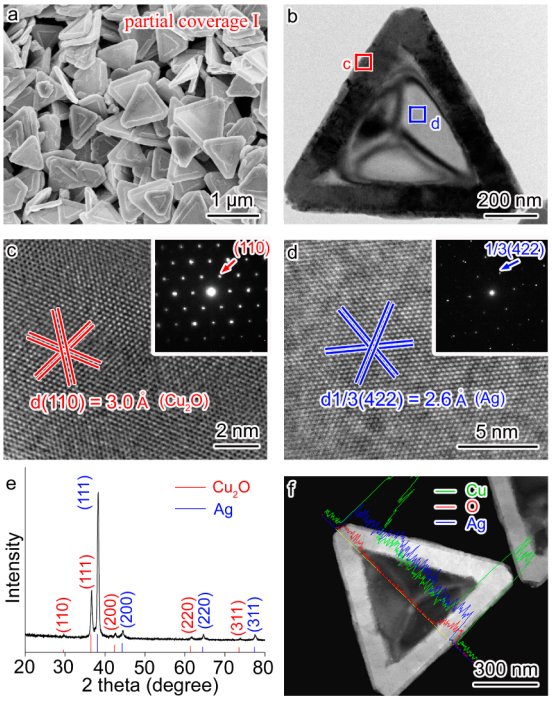

Figure 1. (a) SEM and (b) TEM images of Ag-Cu_2O hybrid structures (partial coverage I). (c, d) HRTEM images taken from the edge and central regions in the image b, respectively. The insets show SAED patterns taken from the corresponding regions. (e) XRD pattern for the partial coverage I sample. (f) EDS line mapping profiles of a Ag-Cu_2O hybrid structure (partial coverage I) along the altitude direction.

the size distribution of Ag nanoplate templates. The structures of edge and central regions in the hybrid structures have been characterized by high-resolution TEM (HRTEM) and selected area electron diffraction (SAED) (Figure 1c,d). The lattice fringes can be well assigned to the {110} of Cu_2O and the 1/3{422} of Ag, respectively, which agree with the SAED patterns. The forbidden 1/3{422} reflection is a characteristic for Ag or Au nanostructures in the form of thin plates or films bounded by atomically flat {111} surfaces.[16−18] These results indicate that the flat faces of Cu_2O and Ag are both bounded by {111} planes, and the Cu_2O has been selectively grown on the edges of the Ag nanoplates. The compositions and phases of hybrid structures are further confirmed by X-ray diffraction (XRD). As shown in Figure 1e, all the diffraction peaks can be assigned to face-centered cubic (fcc) Cu_2O (JCPDS card no. 78-2076) and fcc Ag (JCPDS card no. 65-2871). To identify the specific deposition location of Cu_2O on the Ag nanoplates, we examine the sample by employing energy-dispersive spectroscopy (EDS) line mapping (see Figure 1f). The line mapping profiles along the altitude direction reveal that the addition of Cu_2O is mainly enriched at the edges of the Ag nanoplate.

The interfacial lengths between Ag and Cu_2O in such hybrid structures can be facilely tuned by adjusting the concentrations of $CuCl_2$ precursor added to the synthesis. As the added $CuCl_2$ is increased from 1.6 to 2.4 and 3.2 mg, the Cu_2O growth tends to approach the central region of Ag nanoplates, reducing the interfacial lengths down to 1270 ± 400 and 695 ± 500 nm (namely, partial coverage II and III), respectively (Figures 2a,b and S2−4). When the amount of $CuCl_2$ reaches 4.0 mg, the surface of Ag nanoplates can be fully covered by a single-crystal

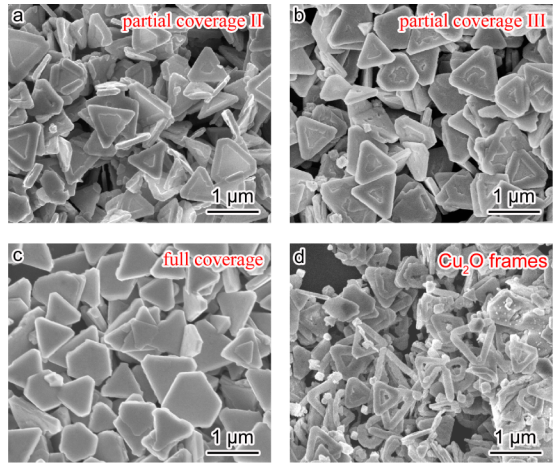

Figure 2. SEM images of (a) Ag-Cu_2O (partial coverage II), (b) Ag-Cu_2O (partial coverage III), (c) Ag-Cu_2O (full coverage), and (d) Cu_2O frames.

Cu_2O layer as long as the PVP is sufficient to stabilize the Cu_2O{111} surface (Figures 2c and S5).

Leveraging the controlled synthesis, we perform catalytic CO oxidation measurements on the samples. In order to evaluate the role of Ag in the CO oxidation, we have prepared a reference sample by removing the Ag from the partial coverage I by KBr etching. As displayed in Figures 2d and S6, the Cu_2O nanostructures appear like frames after the removal of Ag nanoplates despite the existence of trace AgBr byproduct and Ag residue. Prior to the catalytic measurements, we first convert the Cu_2O surface into stable CuO by treating all the samples in a cycle of CO oxidation. After the oxidation, X-ray photoelectron spectra (XPS, Figure S7) identify the Cu^{II} characteristics in the samples, the Cu $2p_{3/2}$ binding energy at 933.3 eV together with a doublet shoulder for the samples, while the Cu^{I} feature completely disappears, demonstrating that the surface of Cu_2O has been turned into CuO. XRD and HRTEM characterizations (Figure S8) confirm that the formed CuO is only present on the surface of Cu_2O. Despite the change in surface composition, the morphologies of samples are largely maintained (Figure S9).

After the first oxidation cycle, all the samples show improved and stable catalytic performance owing to the CuO surface (Figure S10). Fitting the Arrhenius plots (Figure S11), we have acquired their apparent activation energies as listed in Table 1. The data used to plot the Arrhenius plots are of conversions below 10% and within the surface reaction kinetic-controlled region. The full-coverage sample exhibits apparent activation energy of about 62.8 kJ/mol, which agrees well with the value previously observed for the CuO surface that evolves from {111}-covered Cu_2O nanocrystals by oxidation.[7] It suggests that the addition of Ag substrate does not alter the catalytic performance of CuO/Cu_2O(111) catalyst. In stark contrast, all the three hybrid samples with partial coverage show significantly lower apparent activation energies (36.7−42.7 kJ/mol), demonstrating the role of exposed Ag-CuO interface in improving catalytic activities. Note that bare Ag nanoplates show the vanished catalytic activity in the CO oxidation (Figure S1), so the activation sites should not be at the flat surface of Ag. The apparent activation energy of CuO/Cu_2O frames is calculated to be 66.4 kJ/mol, similar to that for the full-coverage sample. The apparent activation energy of a catalytic reaction is a constant whose physical meaning depends on the

dx.doi.org/10.1021/ja506269y | J. Am. Chem. Soc. 2014, 136, 14650−14653

Table 1. Apparent Activation Energies (E_a) of CO Oxidation Catalyzed by Various CuO/Cu_2O-Based Samples Calculated from the Arrhenius Plots Employing the Steady-State CO Conversion Data Measured in the Second Cycle of Catalytic CO Oxidation

sample	partial coverage I	partial coverage II	partial coverage III	full coverage	frames
E_a (kJ mol^{-1})	42.7 ± 1.5	37.0 ± 1.8	36.7 ± 1.3	62.8 ± 2.1	66.4 ± 7.1

detailed reaction mechanism, but it can serve as a useful parameter to distinguish active sites of different catalysts. In particular, the activity trends among our catalysts are the same across all reaction temperatures and CO conversions that we have measured (see Figures S10 and S12). Thus, these results clearly prove that the Ag-CuO interfaces of the three hybrid samples with partial coverage are responsible for the lower apparent activation energies for catalyzing CO oxidation. In other words, the active sites of hybrid structures with partial coverages in catalyzing CO oxidation are more active than those of fully covered CuO/Cu_2O-Ag hybrid structures and CuO/Cu_2O frames.

More interestingly, we have observed strong influence of the lengths of Ag-CuO interfaces on the catalytic performance. Figure S12 summarizes the performance of all the Ag-CuO/Cu_2O samples with partial coverage in the catalytic CO oxidation. The CO conversion rates turn out to decrease in the order of partial coverage I > partial coverage II > partial coverage III at all reaction temperatures. This finding illustrates that increasing the Ag-CuO interfacial length can efficiently promote the catalytic CO oxidation, further confirming that the Ag-CuO interfaces determine the number of active sites.

The information gleaned above has identified the importance of Ag-CuO interface to the CO oxidation. Now we are in a position to elucidate the underlying mechanism. Previous studies suggest that the oxide-metal interface is one of the major factors determining the activity and selectivity of heterogeneous catalysts.[19−22] The difference between the work functions of two materials would drive charge transfer through the interface, consequently altering catalytic reactivity.[23−26] The open question here is how far from the interfacial plane this polarization can affect. To address this issue, we have employed first-principles calculations to examine our material system as illustrated in Figure 3a. In our system, the Cu_2O(111) is first grown on the flat (111) surface of Ag nanoplates. According to the symmetry of fcc lattice,[16−18] the side faces of Cu_2O should be (100). Our XPS characterizations have revealed that the surface of Cu_2O is oxidized into CuO after the first treatment cycle. As a result, the newly formed side CuO layer would be extended to directly interface with Ag(111) substrate (i.e., the region labeled with b in Figure 3a), while the top CuO layer only contacts the Cu_2O(111). To resolve the Ag(111)-CuO interfacial structure, we thus simulate the growth of CuO layer from the Cu_2O(100) side face by optimizing the atomic model for CuO/Cu_2O(100) (Figure S13a). Upon acquiring the optimal CuO surface structure, we analyze the interface between the side CuO layer and the Ag(111) substrate to elucidate the interfacial effect (Figure S13b). Note: (1) the simulation results are consistent regardless of whether the Cu_2O side faces take an undercut or overcut profile; and (2) the CuO/Cu_2O(111) for CO oxidation has been previously calculated,[7] providing a reference value for examining the role of top CuO layer.

The calculated static potential as in Figure S14, taken along the direction perpendicular to Ag(111), suggests charge flow from Ag (higher potential, with work function of 4.45 eV) to CuO (lower potential, with work function of 5.97 eV). To

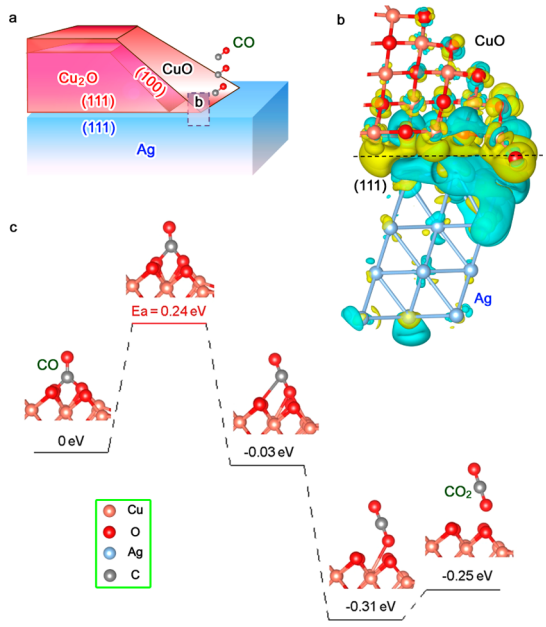

Figure 3. (a) Schematic illustration for the Ag-CuO/Cu_2O hybrid structures (side view for cross section). (b) Atomic model for Ag(111) substrate interfacing with the extension part of side CuO layer (see more models in Figure S13). Differential charge density by first-principles simulations illustrates the increase (olive color) and decrease (cyan color) of electron distributions. (c) Energy profiles of each elementary step in CO oxidation catalyzed by the side CuO layer polarized by the Ag-CuO interface, depicted by first-principles simulations.

better examine this interfacial effect, we have analyzed the differential charge density for Ag(111)-CuO interface. As shown in Figure 3b, a significant increase in electron density (indicated by olive color) has been observed at the CuO surface, along with the reduction of electron density at the interface layer of Ag(111) (cyan color). Due to this polarization effect, CuO is negatively charged leading to the enhancement of CO oxidation, which has been revealed by the simulations for reaction transition states. As displayed in Figure 3c, the transition energy barrier for the side CuO layer polarized by our Ag(111)-CuO interface is as low as 0.24 eV in the CO activation, showing very high oxidation probability at the CuO surface. In stark contrast, the energy barrier is increased to 0.60 eV when the Ag substrate is intentionally removed from the simulation model to exclude the polarization effect (Figure S15). Note that we also consider the possibility of CO adsorption at the Ag-CuO interfacial lines, but the simulations reveal that the CO adsorption cannot be stabilized at the interface as it preferentially occurs on the CuO side. Together with the catalytic comparison of partial coverage samples with CuO/Cu_2O frames, this finding indicates that the surface polarization should be responsible for lowering the activation energy.

From the differential charge density (Figure 3b), one can recognize that the electronic polarization effect dramatically decays with the distance to the Ag(111)-CuO interface. For this

dx.doi.org/10.1021/ja506269y | J. Am. Chem. Soc. 2014, 136, 14650−14653

reason, the CuO/Cu_2O has to partially cover the surface of Ag nanoplates, exposing the side CuO layer for CO oxidation. In the case of full-coverage Ag-CuO/Cu_2O sample, the CuO/Cu_2O layers are too thick to exhibit the polarization effect from the Ag substrates. As such, their activation energy is mainly determined by the electronic structures of $CuO/Cu_2O(111)$. According to previous simulation results,[7] the transition energy barrier for $CuO/Cu_2O(111)$ is 0.37 eV, 0.13 eV higher than that for our Ag(111)-CuO interface. It suggests that the full-coverage sample should display relatively high activation energy, aligning well with our experimental findings (Table 1). Furthermore, this comparison of transition energy barriers shows that the top CuO layer cannot be as catalytically active for CO oxidation as the side CuO in the partial-coverage samples. In this case, their catalytic activities are strongly dependent on the interfacial lengths of Ag(111) and CuO side layer. As only few layers of CuO can receive the polarized charges, the Ag-CuO interfacial lines are the locations to provide high catalytic activity (i.e., the interface acting like one-dimensional material). As a result, the specific CO conversion rates have a strong correlation with the number of active sites along the interfacial lines at all temperatures (Figure S16). This argument is also in agreement with other experimental observations: the thickness of samples follows the sequence of partial coverage I < partial coverage II < partial coverage III (average: 80, 110, and 160 nm, see Figure S17), implying that the thickness is not a key parameter to improving catalytic efficiency. Otherwise, the CO conversion rates would not decrease in the order of partial coverage I > partial coverage II > partial coverage III.

On the other hand, we notice that the adsorption energy of CO on CuO surface slightly decreases from 3.19 to 2.94 eV due to the presence of Ag substrate, suggesting that Ag-CuO polarization does not help attract CO reactants. Meanwhile, simulations reveal that O_2 cannot be adsorbed to the O-riched CuO surface, but Ag surface can capture O_2 with adsorption energy of 0.84 eV that is not altered with the presence of CuO/Cu_2O. Therefore, we conclude that the polarization at the Ag-CuO interface mainly helps lower the reaction energy barrier.

In conclusion, we have been able to better activate the CO oxidation by forming a desirable interface with surface polarization and further improve conversion rates by increasing the number of active sites next to the interface. This work opens up a new strategy for the design of efficient and economic oxide-metal catalysts through interface engineering. It is envisioned that future work with better control over size distributions or combination with ALD technique would further boost catalytic activities.

■ ASSOCIATED CONTENT

Supporting Information

Experimental details and additional material characterizations. This material is available free of charge via the Internet at http://pubs.acs.org.

■ AUTHOR INFORMATION

Corresponding Authors

yjxiong@ustc.edu.cn
jiangj1@ustc.edu.cn
huangwx@ustc.edu.cn

Author Contributions

†These authors contributed equally.

Notes

The authors declare no competing financial interest.

■ ACKNOWLEDGMENTS

This work was financially supported by the 973 Program (no. 2014CB848900), NSFC (no. 21101145, 91123010), Hok Ying Tung Education Foundation (no. 131012), Specialized Research Fund for the Doctoral Program of Higher Education (no. 20123402110050), Recruitment Program of Global Experts, CAS Hundred Talent Program, and Fundamental Research Funds for the Central Universities (nos. WK2060190025, WK2090050027).

■ REFERENCES

(1) Hellman, A.; Klacar, S.; Grönbeck, H. *J. Am. Chem. Soc.* **2009**, *131*, 16636.
(2) Chen, H.; Zhu, W.; Xiao, D.; Zhang, Z. *Phys. Rev. Lett.* **2011**, *107*, 056804.
(3) Long, R.; Mao, K.; Ye, X.; Yan, W.; Huang, Y.; Wang, J.; Fu, Y.; Wang, X.; Wu, X.; Xie, Y.; Xiong, Y. *J. Am. Chem. Soc.* **2013**, *135*, 3200.
(4) Xia, Y.; Xiong, Y.; Lim, B.; Skrabalak, S. E. *Angew. Chem., Int. Ed.* **2009**, *48*, 60.
(5) Xie, X.; Li, Y.; Liu, Z.; Haruta, M.; Shen, W. *Nature* **2009**, *458*, 746.
(6) Huang, W. C.; Lyu, L. M.; Yang, Y. C.; Huang, M. H. *J. Am. Chem. Soc.* **2012**, *134*, 1261.
(7) Bao, H.; Zhang, W.; Hua, Q.; Jiang, Z.; Yang, J.; Huang, W. *Angew. Chem., Int. Ed.* **2011**, *50*, 12294.
(8) Kolpak, A. M.; Grinberg, I.; Rappe, A. M. *Phys. Rev. Lett.* **2007**, *98*, 166101.
(9) Vayenas, C. G.; Bebelis, S.; Ladas, S. *Nature* **1990**, *343*, 625.
(10) Sun, Y. N.; Giordano, L.; Goniakowski, J.; Lewandowski, M.; Qin, Z. H.; Noguera, C.; Shaikhutdinov, S.; Pacchioni, G.; Freund, H. J. *Angew. Chem. Int. Ed.*. **2010**, *49*, 4418.
(11) Yamada, Y.; Tsung, C. K.; Huang, W.; Huo, Z.; Habas, S. E.; Soejima, T.; Aliaga, C. E.; Somorjai, G. A.; Yang, P. *Nat. Chem.* **2011**, *3*, 372.
(12) Kuo, C.-H; Hua, T. E.; Huang, M. H. *J. Am. Chem. Soc.* **2009**, *131*, 17871.
(13) Bai, S.; Ge, J.; Wang, L.; Gong, M.; Deng, M.; Kong, Q.; Song, L.; Jiang, J.; Zhang, Q.; Luo, Y.; Xie, Y.; Xiong, Y. *Adv. Mater.* 10.1002/adma.201401817.
(14) Zhang, Q.; Yang, Y.; Li, J.; Iurilli, R.; Xie, S.; Qin, D. *ACS Appl. Mater. Interfaces* **2013**, *5*, 6333.
(15) Zhang, D.-F; Zhang, H.; Guo, L. *J. Mater. Chem.* **2009**, *19*, 5220.
(16) Kirkland, A. I.; Jefferson, D. A.; Duff, D. G.; Edwards, P. P.; Gameson, I.; Johnson, B. F. G.; Smith, D. J. *Proc. R. Soc. London, Ser. A* **1993**, *440*, 589.
(17) Germain, V.; Li, J.; Ingert, D.; Wang, Z. L.; Pileni, M. P. *J. Phys. Chem. B* **2003**, *107*, 8717.
(18) Xiong, Y.; Siekkinen, A. R.; Wang, J.; Yin, Y.; Kim, M. J.; Xia, Y. *J. Mater. Chem.* **2007**, *17*, 2600.
(19) Boffa, A.; Lin, C.; Bell, A. T.; Somorjai, G. A. *J. Catal.* **1994**, *149*, 149.
(20) Hayek, K.; Fuchs, M.; Klotzer, B.; Reichl, W.; Rupprechter, G. *Top. Catal.* **2000**, *13*, 55.
(21) Park, J. Y.; Renzas, J. R.; Contreras, A. M.; Somorjai, G. A. *Top. Catal.* **2007**, *46*, 217.
(22) Tauster, S. J.; Fung, S. C.; Garten, R. L. *J. Am. Chem. Soc.* **1978**, *100*, 170−175.
(23) Haller, G. L.; Resasco, D. E. *Adv. Catal.* **1989**, *36*, 173.
(24) Schwab, G. M. *Angew. Chem., Int. Ed.* **1967**, *6*, 375.
(25) Somorjai, G. A.; Park, J. Y. *Angew. Chem., Int. Ed.* **2008**, *47*, 9212.
(26) Wang, Y.-G.; Yoon, Y.; Glezakou, V.-A.; Li, J.; Rousseau, R. *J. Am. Chem. Soc.* **2013**, *135*, 10673.